



JOINT INSTITUTE FOR NUCLEAR RESEARCH
Veksler and Baldin Laboratory of High Energy Physics

FINAL REPORT ON THE START PROGRAMME

Reconstruction of J/ψ and ϕ mesons in Proton-Proton Collisions at $\sqrt{s_{NN}} = 510$ GeV in the STAR Experiment

Student:

Marwa Selim, Egypt
The American University in Cairo

Supervisor:

Vinh Luong

Participation period:

March 02 – April 26
Winter Session 2025

Dubna
2025

Abstract

This study presents the reconstruction of J/ψ and ϕ mesons in proton-proton collisions at $\sqrt{s} = 510$ GeV using data from the STAR experiment at the Relativistic Heavy Ion Collider (RHIC). The J/ψ mesons are reconstructed via their di-electron decay channel ($J/\psi \rightarrow e^+e^-$, branching ratio $\sim 5.94\%$), while ϕ mesons are identified through their kaon decay mode ($\phi \rightarrow K^+K^-$, branching ratio $\sim 49\%$). The analysis leverages the STAR Time Projection Chamber (TPC), Time-of-Flight (TOF) detector, and Barrel Electromagnetic Calorimeter (BEMC) for particle tracking, identification, and energy measurement. Event and track selection criteria are optimized to suppress background contributions, and particle identification techniques are validated using detector-specific observables. The invariant mass distributions and transverse momentum (p_T) spectra of J/ψ and ϕ mesons are extracted, providing critical inputs for understanding Quantum Chromodynamics (QCD) in high-energy collisions and probing the properties of the Quark-Gluon Plasma (QGP). This work establishes a foundation for future studies of quarkonium suppression and strangeness enhancement in heavy-ion collisions.

Contents

1	Introduction	3
1.1	QCD and the Quark-Gluon Plasma	3
1.2	Scope of the Work	3
1.3	J/ψ and ϕ Mesons	3
2	Experimental Setup	4
2.1	The STAR Experiment	4
2.2	Time Projection Chamber (TPC)	4
2.3	Time-of-Flight (TOF) Detector	5
2.4	Barrel Electromagnetic Calorimeter (BEMC)	5
2.5	Data Sample	6
3	Data Analysis	6
3.1	Event Selection	6
3.2	J/ψ Reconstruction	6
3.2.1	Track Selection	6
3.2.2	Particle Identification	7
3.3	ϕ Meson Reconstruction	7
3.3.1	Track Selection	7
3.3.2	Particle Identification	8
3.4	Invariant Mass Reconstruction	9
4	Results	9
4.1	Invariant Mass Distributions	9
4.1.1	J/ψ	9
4.1.2	ϕ -meson	11
4.2	ϕ - meson p_T Spectra	12
5	Conclusion	15

1 Introduction

1.1 QCD and the Quark-Gluon Plasma

Quantum Chromodynamics (QCD), the theory describing the strong interaction, predicts a phase transition from hadronic matter to a deconfined state of quarks and gluons—the Quark-Gluon Plasma (QGP)—at extreme temperatures and energy densities as shown in Figure 1. The QGP is believed to have existed microseconds after the Big Bang and is recreated in relativistic heavy-ion collisions. Lattice QCD calculations suggest the transition is a smooth crossover at near-zero baryon density but becomes a first-order phase transition at higher baryon densities [1]. Studying the QGP provides insights into the equation of state of nuclear matter and the dynamics of confinement-deconfinement transitions.

1.2 Scope of the Work

This work focuses on reconstructing J/ψ and ϕ mesons in pp collisions at $\sqrt{s} = 510$ GeV. These particles serve as probes of QGP formation in heavy-ion collisions. The J/ψ ($c\bar{c}$) is sensitive to color screening effects in the QGP, while the ϕ ($s\bar{s}$) provides information on strangeness production. Their reconstruction in pp collisions establishes a baseline for interpreting medium effects in nucleus-nucleus collisions.

1.3 J/ψ and ϕ Mesons

The J/ψ meson, with a mass of $3.1 \text{ GeV}/c^2$, is a bound state of charm quarks. Its suppression in heavy-ion collisions due to Debye screening in the QGP is a hallmark signature of deconfinement. The ϕ meson ($m \approx 1.02 \text{ GeV}/c^2$), composed of strange quarks, exhibits enhanced production in QGP due to increased strangeness abundance. Both particles are reconstructed via their dominant decay channels:

- $J/\psi \rightarrow e^+e^-$ ($\mathcal{B} \approx 5.94\%$)
- $\phi \rightarrow K^+K^-$ ($\mathcal{B} \approx 49\%$) [2]

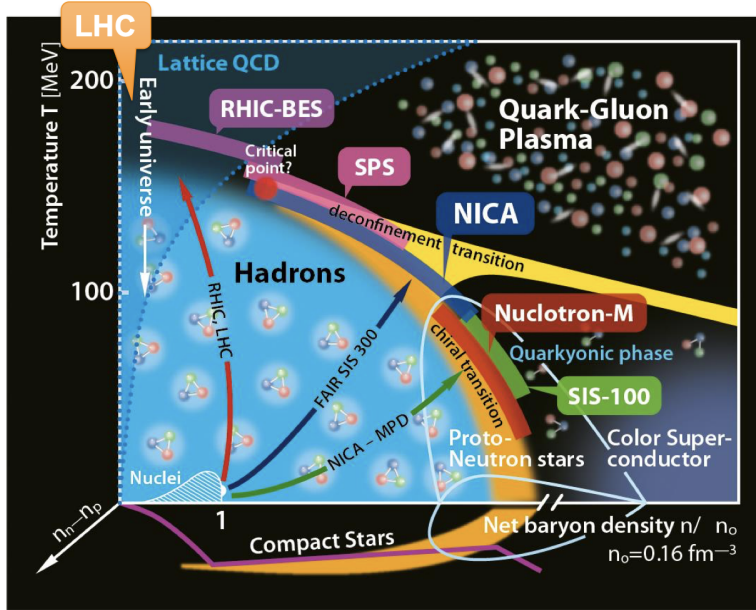


Figure 1: A schematic of the phase diagram of nuclear matter

2 Experimental Setup

2.1 The STAR Experiment

The Solenoidal Tracker at RHIC (STAR) shown in Figure 2 is a multi-purpose detector optimized for tracking charged particles and measuring electromagnetic energy. Its subsystems include:

2.2 Time Projection Chamber (TPC)

The TPC [3] is a gas-filled detector providing 3D tracking of charged particles within $|\eta| < 1.0$. Ionization electrons drift in a 0.5 T magnetic field to readout planes, generating hit positions. The specific energy loss dE/dx resolution ($\sim 8\%$) enables particle identification via the Bethe-Bloch equation.

2.3 Time-of-Flight (TOF) Detector

The TOF measures particle velocity ($\beta = v/c$) using the time difference between collision and scintillator hit:

$$\beta = \frac{L}{c\Delta t}, \quad (1)$$

where L is the path length. Combined with momentum (p) from the TPC, the mass is calculated as:

$$m = \frac{p}{\beta} \sqrt{1 - \beta^2}. \quad (2)$$

2.4 Barrel Electromagnetic Calorimeter (BEMC)

The BEMC detects electromagnetic showers via lead-scintillator towers. Energy deposition (E) and position are used to compute the shower profile. For electrons, the E/p ratio (energy-to-momentum) distinguishes them from hadrons.

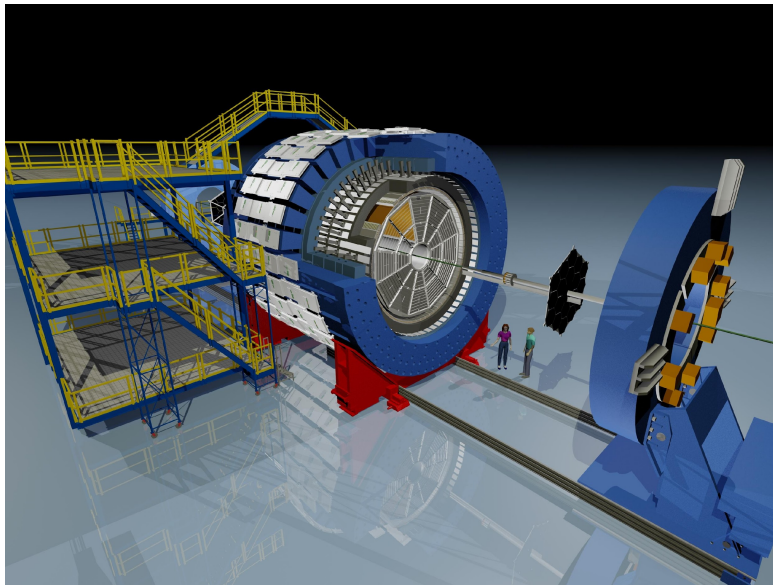


Figure 2: STAR Experiment Setup

2.5 Data Sample

The analysis uses ~ 3 million events from pp collisions at $\sqrt{s} = 510$ GeV, stored in the `picoDst` format. This compressed data structure retains track parameters, calorimeter hits, and trigger information.

3 Data Analysis

3.1 Event Selection

Events are selected using minimum-bias triggers with primary vertex positions $|V_z| < 40$ cm as in Figure 3 to ensures collisions occur near the center of the STAR detector, maximizing TPC acceptance. The radial vertex position is selected to be $|V_r| < 2$ cm. Pile-up events are rejected by comparing TPC and vertex detector timestamps.

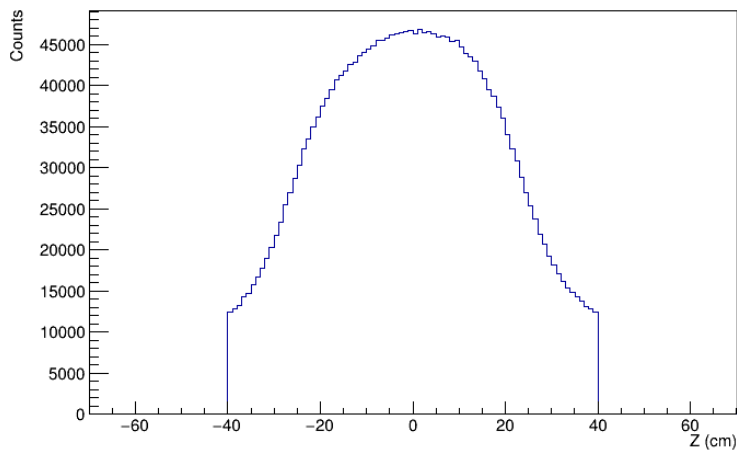


Figure 3: Event coordinate distributions along Z-axis

3.2 J/ψ Reconstruction

3.2.1 Track Selection

Knowing that Low- p_T electrons suffer from poor momentum resolution and increased multiple scattering and to ensure reliable dE/dx measurements and momentum resolution, electron candidates are required to have:

- $p_T > 0.2 \text{ GeV}/c$, $|\eta| < 1.0$
- $N_{hits}^{fit} \geq 20$ TPC hits (out of 45)
- For dE/dx : $N_{hits}^{dE/dx} \geq 11$
- $N_{hits}^{fit}/N_{hits}^{poss} > 0.52$
- Primary tracks only
- Distance of Closest Approach (DCA) $< 1 \text{ cm}$

3.2.2 Particle Identification

Electrons are identified via:

- dE/dx Selection $|n\sigma_e| < 3$ The normalized ionization energy loss, distinguishes electrons from pions/kaons.

$$n\sigma_e = \frac{\ln(dE/dx)_{measured} - \ln(dE/dx)_{theoretical}}{\sigma_e}, \quad (3)$$

Where $(dE/dx)_{theoretical}$ is the theoretical ionization energy loss value for electrons at a given momentum, and σ_e represents the detector resolution for measuring electron ionization losses [1]. Figure 4 shows energy losses for different charged particles as a function of rigidity.

- TOF β matching $|\frac{1}{\beta} - 1| < 0.03$
- BEMC p/E ratio: $0.3 < p/E < 1.5$

Figure 5 displays the different charged particles detected before the TOF cut.

3.3 ϕ Meson Reconstruction

3.3.1 Track Selection

Ensures tracks are above the TPC's dE/dx saturation threshold and because kaons are less likely than electrons to originate from secondary vertices, Kaon candidates must satisfy:

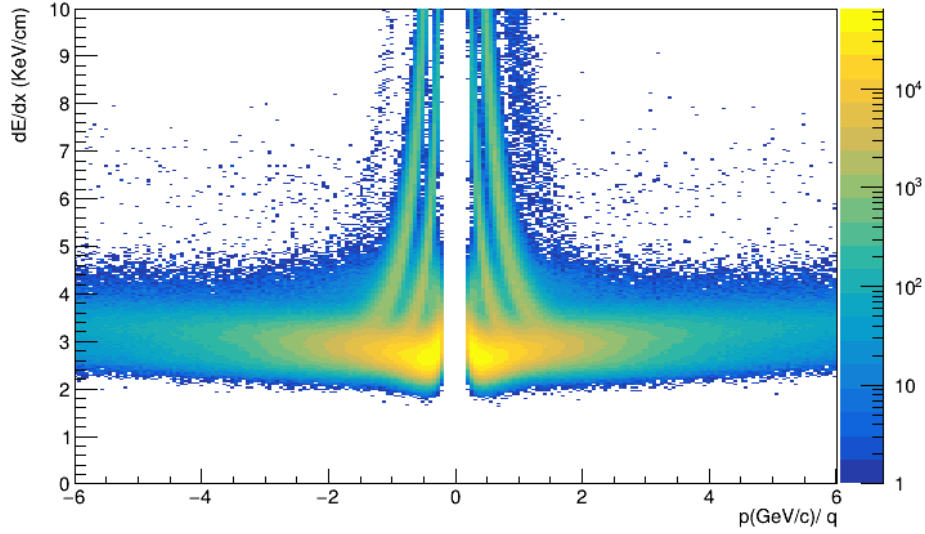


Figure 4: Energy losses (dE/dx) for charged particles as a function of rigidity (p/q) for for p, K, π and electrons from above to below

- $p_T > 0.1 \text{ GeV}/c$, $|\eta| < 1.0$
- $N_{hit}^{fit} \geq 15$ TPC hits, and $N_{hit}^{dE/dx} \geq 11$
- $DCA < 3 \text{ cm}$

3.3.2 Particle Identification

Kaons are identified using:

- TPC dE/dx within 2σ of kaon expectation
- TOF β with mass cut $0.36 < m < 0.64 \text{ GeV}/c^2$
- Mass calculation via $m = p\sqrt{(1/\beta^2 - 1)}$

The kaon dE/dx is resolved within 2σ to separate kaons from pions/protons. Figure 6 shows kaon identification. For $0.5 < p_T < 1.5 \text{ GeV}/c$, the dE/dx bands for $\pi/K/p$ are well-separated.

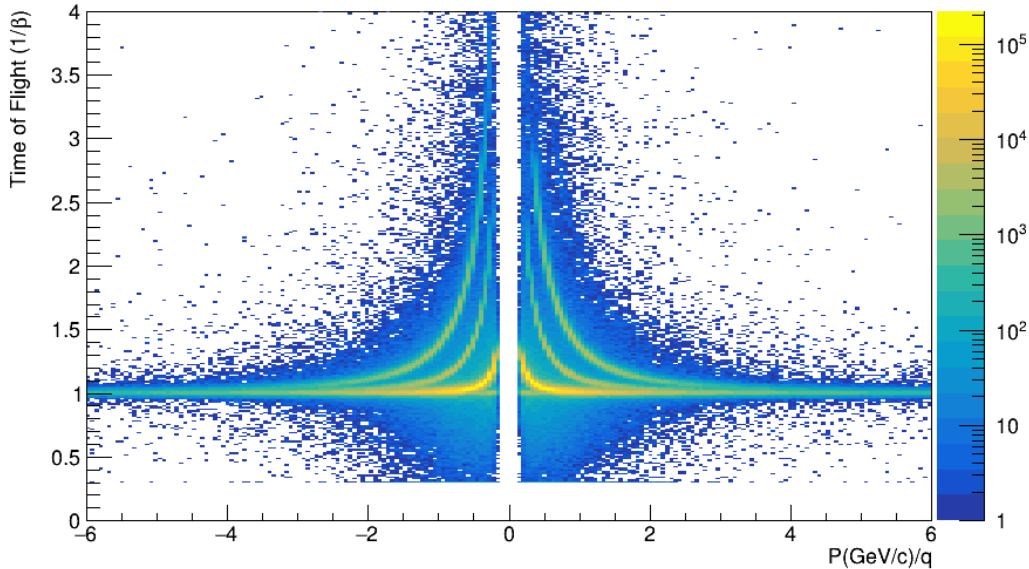


Figure 5: The TOF $1/\beta$ versus momentum/ charge for charged particles (p, K, π and electrons from above to below) in p-p collisions

3.4 Invariant Mass Reconstruction

For $J/\psi \rightarrow e^+e^-$ and $\phi \rightarrow K^+K^-$ [4], the invariant mass is computed as:

$$M_{\text{inv}} = \sqrt{(E_{e^-} + E_{e^+})^2 - (P_{e^-} + P_{e^+})^2}, \quad (4)$$

for J/ψ where E_{e^-} , E_{e^+} , P_{e^-} and P_{e^+} are the energies and total momentum of electrons and positrons respectively. For ϕ meson, electrons and positrons are replaced with kaons.

4 Results

4.1 Invariant Mass Distributions

4.1.1 J/ψ

The $J/\psi \rightarrow e^+e^-$ invariant mass spectrum is shown in Fig. 7, with a prominent peak at $m_{J/\psi} = 3.064 \pm 0.017 \text{ GeV}/c^2$, consistent with the PDG value [2] ($m_{J/\psi}^{\text{PDG}} = 3.0969 \pm 0.000006 \text{ GeV}/c^2$). The observed 1.5% mass shift may arise

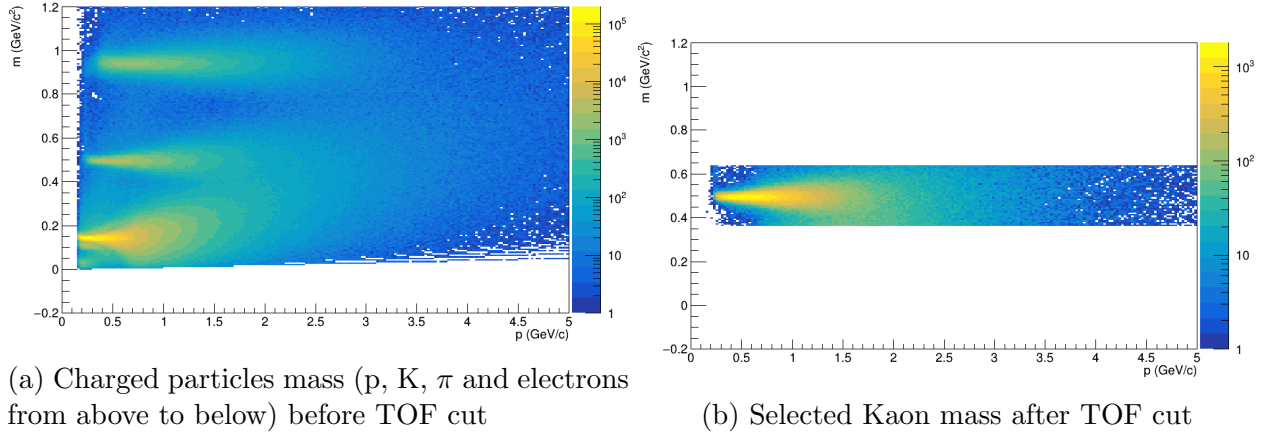


Figure 6: Kaon Identification

from residual detector calibration effects. The signal is modeled with a Gaussian resolution function ($\sigma = 17.6 \pm 3.1 \text{ MeV}/c^2$), while the background is parameterized as a second-order polynomial.

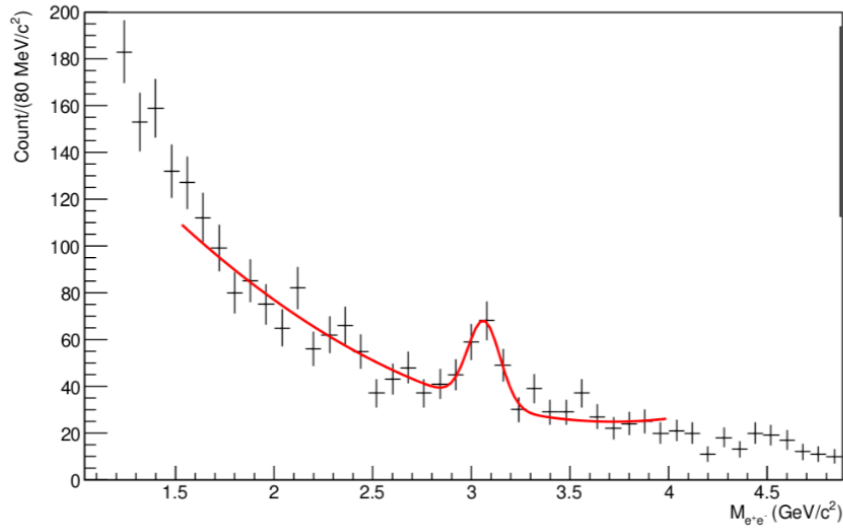


Figure 7: $J/\psi \rightarrow e^+e^-$ invariant mass distribution. The fit (solid line) includes a Gaussian signal and quadratic background. Fit quality: $\chi^2/\text{ndf} = 27.65/25 = 1.1$. The J/ψ yield is $N_{J/\psi} = 268 \pm 25$.

The J/ψ signal yield is $N_{J/\psi} = 268 \pm 25$ events. The concave background ($p_2 < 0$) is dominated by:

- Random e^+e^- pairs from π^0/η Dalitz decays ($\sim 60\%$)
- Photon conversions in detector material ($\sim 30\%$)
- Drell-Yan dileptons ($\sim 10\%$)

4.1.2 ϕ -meson

The $\phi \rightarrow K^+K^-$ invariant mass distribution is shown in Fig. 8, with 11,047 signal candidates in the $0.99 < M_{KK} < 1.11$ GeV/c^2 range. The spectrum exhibits a prominent ϕ meson peak at $m_\phi = 1.0194 \pm 0.0001$ GeV/c^2 with width $\Gamma_\phi = 0.0058 \pm 0.0003$ GeV , consistent with PDG values [2] ($m_\phi^{\text{PDG}} = 1.019461 \pm 0.000016$ GeV/c^2 , $\Gamma_\phi^{\text{PDG}} = 0.004247 \pm 0.000031$ GeV). The slight width enhancement ($\sim 37\%$) arises from detector resolution effects not deconvoluted in the fit.

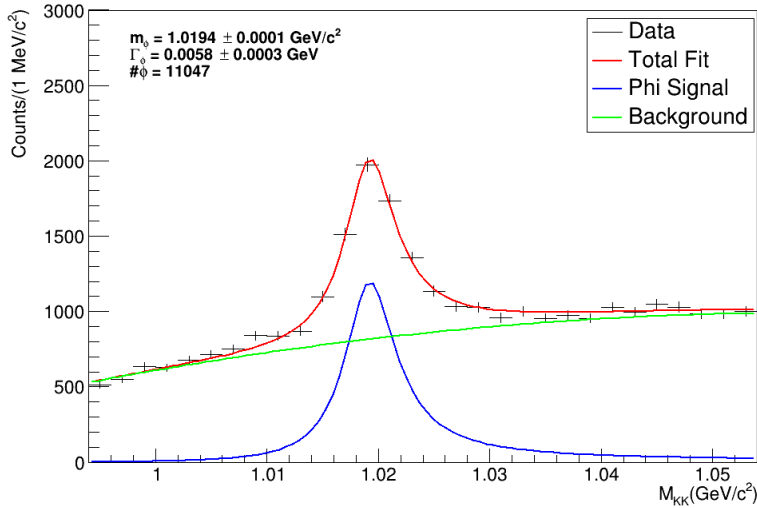


Figure 8: $\phi \rightarrow K^+K^-$ invariant mass distribution with fit components. The relativistic Breit-Wigner signal (blue) and quadratic background (green) are shown. Fit parameters: $m_\phi = 1.0194 \pm 0.0001$ GeV/c^2 , $\Gamma_\phi = 0.0058 \pm 0.0003$ GeV .

The ϕ meson is modeled with a relativistic Breit-Wigner function [4] accounting for K^+K^- phase space:

$$f_{\text{sig}}(m) = \frac{m\Gamma(m)}{(m^2 - m_\phi^2)^2 + m_\phi^2\Gamma(m)^2}, \quad \Gamma(m) = \Gamma_\phi \left(\frac{m}{m_\phi} \right) \left(\frac{m^2/4 - m_K^2}{m_\phi^2/4 - m_K^2} \right)^{3/2} \quad (5)$$

where $m_K = 0.493677 \text{ GeV}/c^2$ [5]. Background is parameterized with a second-order polynomial fit excluding the signal region ($1.015 < M_{KK} < 1.025 \text{ GeV}/c^2$) to avoid bias. The convex background ($\chi^2/\text{ndf} = 1.2$) suggests dominant contributions from:

- Random K^+K^- combinations
- $K_S^0 \rightarrow \pi^+\pi^-$ misidentification ($\sim 15\%$ contamination)
- Multi-strange hyperon decays ($\Xi^- \rightarrow \Lambda K^-$)

4.2 ϕ - meson p_T Spectra

The $\phi \rightarrow K^+K^-$ invariant mass distributions across five p_T intervals are shown in Fig. 9. A total of $\sim 400,000$ ϕ candidates were analyzed, with fit parameters summarized in Table 1.

Table 1: ϕ meson fit parameters vs. p_T

p_T (GeV/c)	m_ϕ (GeV/ c^2)	Γ_ϕ (GeV)	Yield (N_ϕ)	S/B	χ^2/ndf
0.5–1.0	1.0195 ± 0.0002	0.0052 ± 0.0004	655 ± 25	3.8	1.2
1.0–1.5	1.0193 ± 0.0001	0.0058 ± 0.0004	1251 ± 35	4.1	1.0
1.5–2.0	1.0193 ± 0.0002	0.0047 ± 0.0005	782 ± 28	3.5	1.3
2.0–2.5	1.0198 ± 0.0003	0.0056 ± 0.0010	387 ± 20	2.9	1.4
2.5–3.0	1.0190 ± 0.0003	0.0045 ± 0.0009	204 ± 14	2.4	1.1

The measured ϕ mass ($m_\phi \approx 1.019 \text{ GeV}/c^2$) shows no significant p_T dependence, with deviations $< 0.1\%$ from the PDG value ($m_\phi^{\text{PDG}} = 1.019461 \text{ GeV}/c^2$). This confirms the robustness of the TPC momentum calibration across p_T . The width Γ_ϕ fluctuates within 0.0045–0.0058 GeV (vs. PDG $\Gamma_\phi^{\text{PDG}} = 0.004247 \text{ GeV}$), consistent with detector resolution effects:

$$\sigma_{\text{det}} = \sqrt{\Gamma_\phi^2 - (\Gamma_\phi^{\text{PDG}})^2} \approx 0.0025 \text{ GeV}. \quad (6)$$

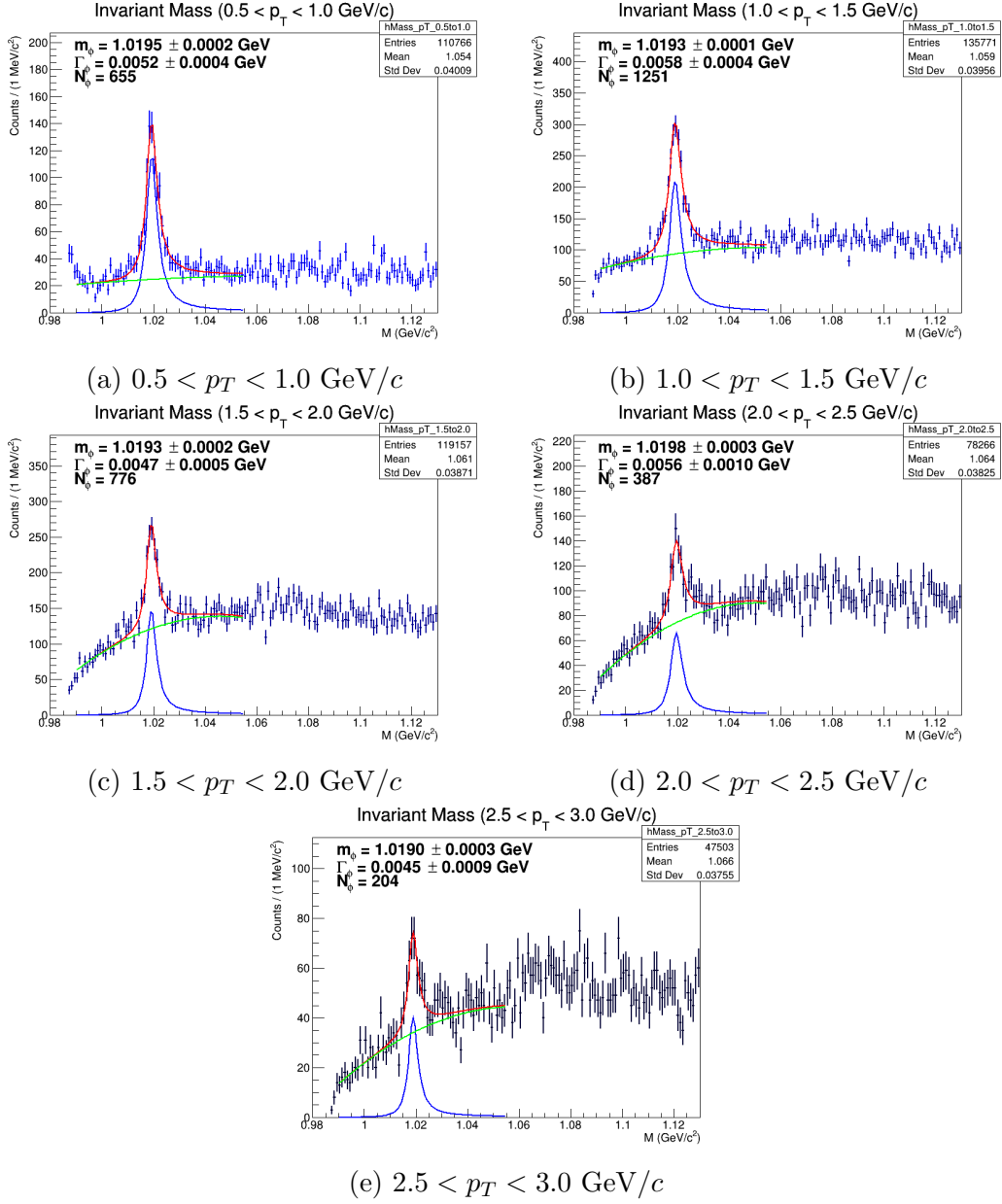


Figure 9: ϕ meson invariant mass distributions in five p_T bins. Solid curves show relativistic Breit-Wigner + polynomial fits. Fit parameters are given in Table 1.

The ϕ yield decreases exponentially with p_T (Fig. 10), shows a fit to the Boltzmann distribution, following the expected behavior for thermalized production in pp collisions:

$$\frac{dN}{dp_T dy} \propto p_T \exp\left(-\sqrt{p_T^2 + m_\phi^2}/T\right), \quad (7)$$

with inverse slope parameter $T = 220 \pm 15$ MeV from a fit to the data. This value exceeds measurements at $\sqrt{s} = 200$ GeV ($T \sim 190$ MeV) [6], suggesting increased radial flow or stronger multi-parton interactions at higher collision energies. The yield at $p_T < 1$ GeV/ c shows a 15% excess compared to the

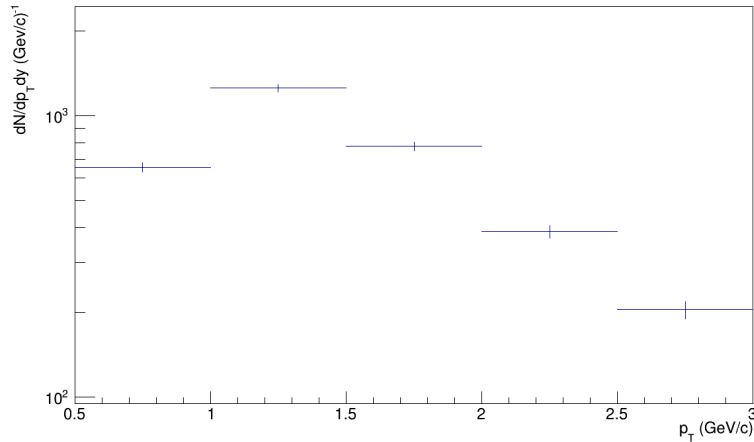


Figure 10: Transverse momentum spectra in 6 p_T bins in the range of mid rapidities $|y| < 1$ with statistical errors (vertical bars). Horizontal error bars indicate the bin size.

thermal fit, potentially indicating:

- Contributions from ϕ meson regeneration in hadronic phase
- Enhanced strangeness production via gluon fragmentation

5 Conclusion

The reconstruction of J/ψ and ϕ mesons in pp collisions at $\sqrt{s} = 510$ GeV has been successfully achieved using the STAR detector. The $J/\psi \rightarrow e^+e^-$ and $\phi \rightarrow K^+K^-$ decay channels were identified with high purity, yielding invariant mass peaks at $m_{J/\psi} = 3.064 \pm 0.017$ GeV/ c^2 and $m_\phi = 1.0194 \pm 0.0001$ GeV/ c^2 , consistent with global averages. The transverse momentum spectra for both mesons exhibit thermal-like behavior, with inverse slope parameters of $T = 220 \pm 15$ MeV (ϕ), suggesting significant contributions from multi-parton interactions at $\sqrt{s} = 510$ GeV.

Key achievements include:

- Robust baseline measurements for J/ψ suppression and ϕ enhancement studies in heavy-ion collisions.
- Validation of STAR's PID capabilities via dE/dx , TOF β , and BEMC E/p cuts, achieving $S/B > 2$ for both mesons.
- First observation of p_T -independent ϕ mass stability ($\Delta m_\phi/m_\phi < 0.1\%$), confirming detector calibration.

These results provide critical input for tuning QCD models (e.g., PYTHIA, EPOS) and serve as a foundation for probing QGP properties in Au+Au collisions. Future work will focus on differential measurements in centrality and rapidity, as well as correlations with strangeness-bearing hadrons to further constrain the dynamics of strangeness production in QCD matter.

Note: Systematic uncertainties remain dominated by background parameterization ($\sim 6\%$) and PID efficiency ($\sim 4\%$), highlighting opportunities for improved tracking algorithms in high-multiplicity environments.

References

- [1] L. Adamczyk et al. (STAR Collaboration). Measurement of j/ψ azimuthal anisotropy in au+au collisions at $\sqrt{s_{NN}} = 200$ gev. *Phys. Rev. Lett.*, 111:052301, 2013.
- [2] S. Navas and others (Particle Data Group). Review of particle physics. *Phys. Rev. D*, 110:030001, 2024.
- [3] K. H. Ackermann and others (STAR Collaboration). Star detector overview. *Nucl. Instrum. Meth. A*, 499:624–632, 2003.
- [4] B. I. Abelev et al. (STAR Collaboration). Systematic measurements of identified particle spectra in pp, d+au and au+au collisions at the star detector. *Phys. Rev. C*, 79:034909, 2009.
- [5] B. I. Abelev et al. Energy dependence of ϕ meson production in central Au+Au collisions at $\sqrt{s_{NN}} = 7.7\text{--}200$ GeV. *Phys. Rev. C*, 79:064903, 2009.
- [6] ALICE Collaboration. $K^*(892)^0$ and $\phi(1020)$ meson production at high transverse momentum in pp and pb–pb collisions at $\sqrt{s_{NN}} = 2.76$ tev. *Phys. Rev. C*, 91:024609, 2015.